September 6, 2012

Large excitonic effects in monolayers of molybdenum and tungsten dichalcogenides

Ashwin Ramasubramaniam, *University of Massachusetts - Amherst*

Large excitonic effects in monolayers of molybdenum and tungsten dichalcogenides

Ashwin Ramasubramaniam*

Department of Mechanical and Industrial Engineering, University of Massachusetts Amherst, Amherst, Massachusetts 01003, USA

(Received 3 July 2012; published 6 September 2012)

Quasiparticle band structures and optical properties of MoS_2, $MoSe_2$, $MoTe_2$, WS_2, and WSe_2 monolayers are studied using the GW approximation in conjunction with the Bethe-Salpeter equation (BSE). The inclusion of two-particle excitations in the BSE approach reveals the presence of two strongly bound excitons (A and B) below the quasiparticle absorption onset arising from vertical transitions between a spin-orbit-split valence band and the conduction band at the K point of the Brillouin zone. The transition energies for monolayer MoS_2, in particular, are shown to be in excellent agreement with available absorption and photoluminescence measurements. Excitation energies for the remaining monolayers are predicted to lie in the range of 1–2 eV. Systematic trends are identified for quasiparticle band gaps, transition energies, and exciton binding energies within as well as across the Mo and W families of dichalcogenides. Overall, the results suggest that quantum confinement of carriers within monolayers can be exploited in conjunction with chemical composition to tune the optoelectronic properties of layered transition-metal dichalcogenides at the nanoscale.

DOI: 10.1103/PhysRevB.86.115409 PACS number(s): 73.22.−f

Layered transition-metal dichalcogenides (LTMDs)—a class of materials in which covalently bound layers are stacked together by van der Waals forces[1–3]—are a rich source of two-dimensional (2D) crystals.[4–7] There has been a resurgence of interest in the properties of these materials, specifically in their 2D crystalline form, for nanoscale electronics and photonics applications.[8–14] For example, monolayer MoS_2 has been employed successfully in the fabrication of low-power field-effect transistors,[12] logic circuits,[13] and phototransistors.[14]

In their bulk states, MoX_2 and WX_2 (X = S, Se, Te) LTMDs are indirect-gap semiconductors.[15,16] It is well documented in the case of MoS_2, through both theory[17,18] and experiment,[9,11,19] that the material remains an indirect-gap semiconductor until samples are thinned down to a monolayer, at which point the gap becomes direct. This is typically evidenced by the emergence of strong photoluminescence (PL) in the monolayer.[9,11,19] The optical spectrum of the monolayer is characterized by the presence of two low-energy exciton peaks that arise from vertical transitions at the K point of the Brillouin zone from a spin-orbit-split valence band to a doubly degenerate conduction band[9,11] [Fig. 1(b)]. These excitons are confined to a (near) 2D geometry and are strongly bound [∼0.9 eV (Ref. 20)] due to poor dielectric screening in the monolayer. While similar PL studies have yet to be performed for other LTMDs, computational studies[21,22] indicate that these materials also remain indirect-gap semiconductors down to bilayer thicknesses and then undergo an indirect-to-direct gap transition upon thinning down to a monolayer. Based on broad similarities in electronic structure within this class of LTMDs, as well as the expected decrease in dielectric screening in monolayer samples, it might be expected that strong excitonic effects are manifested in all monolayer samples of these materials, which could then offer unique possibilities for optoelectronics.

The purpose of this paper is to present a detailed characterization of the electronic band structure and optical properties of MoX_2 and WX_2 monolayers via first-principles calculations. Specifically, the goal here is to accurately predict quasiparticle band structures and optical spectra, which are directly accessible through experimental techniques such as photoemission, photoabsorption, and photoluminescence spectroscopy. It is well known that density functional theory (DFT) is ill equipped to describe photoemission as the Kohn-Sham energies do not formally correspond to quasiparticle energies, which are required to correctly describe electron addition or removal events.[23] A widely-employed and efficient means to overcome this problem is the GW approximation,[24–27] which goes beyond the mean-field, independent-particle DFT approach and properly accounts for many-body electron-electron interactions. While this quasiparticle picture is generally sufficient to obtain accurate photoemission spectra, it is still inadequate for photoabsorption processes[23,28,29] in which electron-hole pairs are created (without actual addition or removal of electrons). This deficiency can be overcome by first treating the quasielectron and quasihole (e.g., within the GW approximation) and then accounting for their interaction by solving the Bethe-Salpeter equation (BSE) for the two-particle Green's function.[23,28,29] While each additional level of theory in the DFT-GW-BSE ladder inevitably increases computational cost, this process cannot be dispensed with for the LTMDs of interest here, given the preexisting evidence for strong exciton binding in MoS_2.[20] Therefore, this sequence of calculations is systematically undertaken for each LTMD monolayer in the following.

Standard Kohn-Sham DFT calculations with the Perdew-Burke-Ernzerhof (PBE) exchange-correlation functional[30] were first performed for structural relaxation of the LTMD monlayers. This was followed by a hybrid-DFT calculation with the Heyd-Scuseria-Ernzerhof (HSE) exchange-correlation functional[31] to obtain eigenvalues and wave functions for the GW calculation. Full-frequency-dependent GW calculations[27] were performed at the non-self-consistent G_0W_0 level, which involves only calculation of quasiparticle energies while preserving the input wave functions. Quasiparticle band structures, dielectric constants, and effective carrier masses were obtained at this point for simple analytical estimates of exciton binding energies. As a final step, BSE calculations were performed in the basis of free quasielectron-quasihole

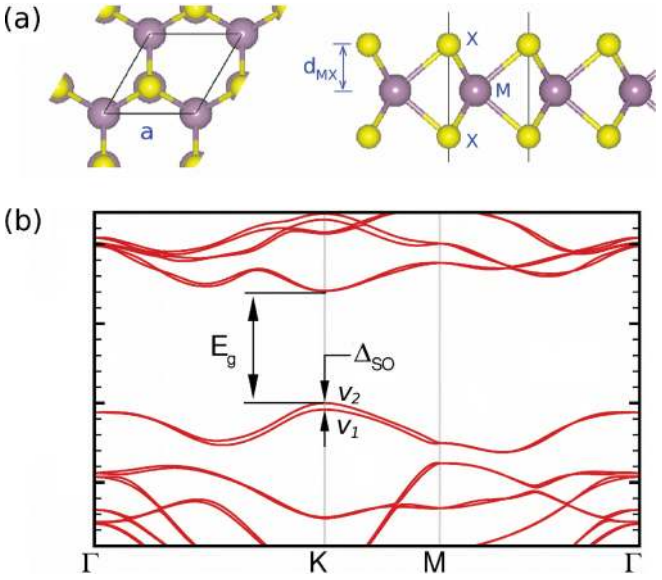

FIG. 1. (Color online) (a) Schematic of $2H_b$ polytype of an MX_2 monolayer (M = metal; X = chalcogen). The unit cell is enclosed by solid lines. (b) Typical band structure for an MX_2 monolayer. The valence-band maximum is split due to spin-orbit coupling. Transitions between v_2 and the conduction-band minimum at K lead to A-type excitons in the absorption spectrum, while transitions between v_1 and the conduction-band minimum at K lead to B-type excitons.

pairs to obtain optical absorption spectra within the Tamm-Dancoff approximation[23] for the monolayer samples. Additional details are provided in the Appendix at the end of this paper. A remark on the intermediate HSE step is in order here: while this step is not essential (i.e., PBE wave functions and eigenvalues can be directly used as inputs for the GW calculation), the computed PL spectrum for MoS_2 was found to be in better agreement with experiments upon inclusion of this step. This is likely because incorporation of a fraction of exact exchange within the HSE functional reduces self-interaction errors, leading to a better description of electronic wave functions.[32] Indeed, the HSE functional has been shown to systematically approximate the optical gap in several instances.[33] At any rate, based on the success of this strategy for reproducing the experimental absorption spectrum for MoS_2, the same procedure is systematically employed for all LTMDs studied here.

We begin by discussing the case of monolayer MoS_2, which has been well characterized experimentally,[9,11,19] thus providing a benchmark for computational studies. All LTMDs considered here commonly crystallize in the $2H_b$ polytype. The corresponding unit cell for a monolayer is displayed in Fig. 1(a); the relevant structural parameters, which are all in excellent agreement with previous studies,[21,34] are listed in Table I. As noted before, the valence-band edge is split due to spin-orbit coupling, the splitting being largest at the K point of the Brillouin zone [Figs. 1(b) and 3]. The conduction-band minimum, which is also at K, is doubly degenerate. Optical transitions between the split valence band and the conduction band give rise to two distinct low-energy peaks in the absorption spectrum, commonly referred to as the A and B excitons.[35] At the PBE level, the valence band undergoes a spin-orbit splitting of 146 meV, which is in excellent agreement with previous calculations.[20,21] The spin-orbit splitting is sensitive to the level of theory employed, following the trend $\Delta_{SO}^{\mathrm{PBE}} < \Delta_{SO}^{\mathrm{G_0W_0}} < \Delta_{SO}^{\mathrm{HSE}}$. Band gaps for various levels of theory are also reported in Table I along with experimental PL gaps. The measured optical gap of 1.8–1.9 eV for MoS_2 is clearly underestimated by the PBE calculations (1.6 eV). The G_0W_0 quasiparticle gap on the other hand is nearly 1 eV in excess of the measured optical gap. Interestingly, the HSE gap is about 0.15–0.2 eV in excess of the optical gap, as also noted in previous work,[36] pointing to the aforementioned tendency of the HSE functional to approximate the optical gap in general.[33] We also note, parenthetically, that the G_0W_0 gap is direct at K, in agreement with the self-consistent GW calculations of Ref. 20.

To enable more direct comparison with experiments, we consider next the absorption spectrum of monolayer MoS_2. Figure 2 displays the imaginary part of the frequency-dependent transverse dielectric constant, $\epsilon_2^{\perp}(\omega)$, in the long-wavelength limit $\boldsymbol{q} \to \mathbf{0}$, which corresponds to interaction with an electromagnetic wave polarized in the plane of the monolayer. Computational results for $\epsilon_2^{\perp}(\omega)$ are displayed for HSE and G_0W_0 calculations (both in the random-phase approximation) as well as for BSE calculations in the Tamm-Dancoff approximation. For comparison, the experimental absorption spectrum from Ref. 9 is also reproduced in Fig. 2. From these data, we see that the G_0W_0 absorption onset is

TABLE I. Structural parameters, valence-band spin-orbit splitting (Δ_{SO}) at K, and direct electronic band gaps (E_g) at K for various LTMD monolayers. (See Fig. 1 for schematic definitions of the tabulated parameters.)

	Structural parameters (Å)		Δ_{SO} (meV)			E_g (eV)			
	a	d_{MX}	PBE	HSE	G_0W_0	PBE	HSE	G_0W_0	Expt. (PL)
MoS_2	3.18	1.56	146	193	164	1.60	2.05	2.82	1.88,[a] 1.85[b]
$MoSe_2$	3.32	1.67	183	261	212	1.35	1.75	2.41	
$MoTe_2$	3.55	1.81	216	344	266	0.95	1.30	1.77	
WS_2	3.19	1.57	425	521	456	1.56	1.87	2.88	
WSe_2	3.32	1.68	461	586	501	1.19	1.68	2.42[c]	

[a]Reference 9; absorption measurement.
[b]Reference 11; PL measurement.
[c]This direct gap at K is not the lowest quasiparticle gap at the G_0W_0 level; the actual gap is 2.34 eV and is indirect, as seen from Fig. 3. At the PBE and HSE level though, the gap is direct at K.

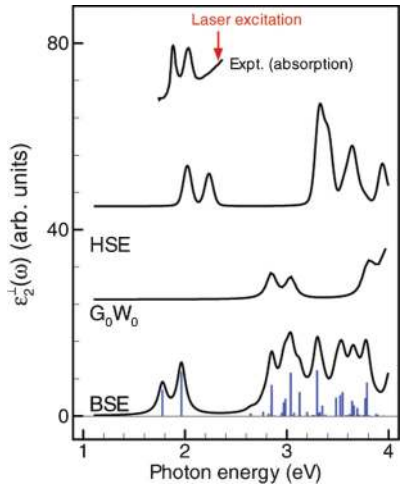

FIG. 2. (Color online) Imaginary part of transverse dielectric constant for monolayer MoS_2, $\epsilon_2^{\perp}(\omega)$, as a function of photon energy ($\hbar\omega$). Computed spectra are presented for three levels of theory: HSE functional, G_0W_0, and BSE. Vertical (blue) bars represent the relative oscillator strengths for the optical transitions. The two lowest-energy peaks in the spectrum (first two bars) correspond to the *A* and *B* excitons. The experimental absorption spectrum for MoS_2 is extracted from Fig. 4 of Ref. 9. (The heights of experimental peaks are arbitrarily rescaled to appear on the same scale as the computational results.) As seen, the closest agreement with experiments is obtained at the level of BSE calculations.

nearly 1 eV higher in energy than the experimental results. However, upon inclusion of electron-hole interactions within the BSE approach, we see the appearance of two distinct absorption peaks at 1.78 and 1.96 eV, which correspond to the strongly bound *A* and *B* excitons, respectively. The positions of these peaks are in excellent quantitative agreement with experiments, as confirmed by the values listed in Table II. These results therefore provide direct evidence for strong exciton binding in the MoS_2 monolayer, which was previously inferred in Ref. 20 using the classical Mott-Wannier model in conjunction with GW calculations. For completeness, we also note that the positions of the HSE absorption peaks for *A* and *B* transitions are in excess of the experimental values by 0.15–0.2 eV. Overall, we conclude that the HSE-G_0W_0-BSE ladder, as employed here, is clearly capable of providing accurate absorption spectra for monolayer MoS_2, which gives us some confidence in using this approach for the other LTMDs of interest. In particular, the Tamm-Dancoff approximation, which has been found to break down for confined systems such as π-conjugated molecules and carbon nanotubes,[37] appears to render sufficiently accurate results for our present purposes.

Before proceeding to the remaining LTMDs, it is useful to consider the exciton binding problem in monolayer MoS_2 (Ref. 20) in the context of the classical Mott-Wannier model. For simplicity, we treat the monolayer as an idealized 2D sheet and assume direct optical transitions between nondegenerate, parabolic bands at *K*. As is well known, the exciton binding energy in 3D is given by $E_b^{3D} = 13.6\mu_{ex}/m_0\epsilon^2$ (in eV), where $\mu_{ex} = m_e m_h/(m_e + m_h)$ is the effective exciton mass, m_0 is the electron mass, and ϵ is the relative dielectric constant;[38] this result is modified in 2D as $E_b^{2D} = 4E_b^{3D}$.[39] The effective electron and hole masses m_e and m_h can be determined from the curvatures of the energy bands at the *K* point and are tabulated in Table II—for simplicity we use the average of the curvatures along the ΓK and KM directions here, which is reasonable given the inherent level of approximation of the model. For comparison, the carrier masses from quasiparticle self-consistent GW (QSGW) calculations of Ref. 20 are also listed in Table II and are seen to be consistently smaller than those obtained from G_0W_0 calculations in this work. It is unclear as yet whether these discrepancies arise primarily from self-consistency (QSGW) or lack thereof (G_0W_0), due to more fundamental differences in the electronic-structure methods employed (pseudopotentials, exchange-correlation functionals, etc.) and merits further investigation. The transverse component of the macroscopic static dielectric tensor for the monolayer, on the other hand, is found to be $4.26\epsilon_0$, which is in excellent agreement with Ref. 20; this value is

TABLE II. Data from G_0W_0 and BSE calculations for various monolayers. The transverse component of the macroscopic static dielectric tensor ($\epsilon_{mac}^{\perp}$) and carrier masses at the *K* point (in units of the electron mass m_0) are determined from G_0W_0 calculations. Analytical estimates of transition energies for *A* excitons are determined by subtracting the Mott-Wannier exciton binding energy from the G_0W_0 band gaps in Table I. BSE data are obtained *ab initio*.

	$\epsilon_{mac}^{\perp}$	Effective mass (m_0)			Mott-Wannier model	BSE transition energy (eV)	
		m_e	m_h	μ_{ex}	Transition energy (eV)	A_1	B_1
MoS_2	4.26	0.60	0.54	0.28	1.97	1.78	1.96
	(4.2[a])	(0.35[a])	(0.44[a])	(0.19[a])	(1.86[a])	(1.88[b], 1.85[c])	(2.03[b], 1.98[c])
$MoSe_2$	4.74	0.70	0.55	0.31	1.66	1.50	1.75
$MoTe_2$	5.76	0.69	0.66	0.36	1.22	1.06	1.36
WS_2	4.13	0.44	0.45	0.22	2.17	1.84	2.28
WSe_2[d]	4.63	0.53	0.52	0.26	1.75	1.52	2.00

[a]Reference 20; self consistent GW calculation. Carrier masses listed here are averages of the longitudinal and transverse values reported in Ref. 20.

[b]Reference 9; absorption measurement.

[c]Reference 11; PL measurement.

[d]Only the effective masses and transition energy from the Mott-Wannier model at the *K* point are calculated here. A proper description of the transition across the true band gap from *K* to 0.52Γ-*K* requires inclusion of electron-phonon coupling.

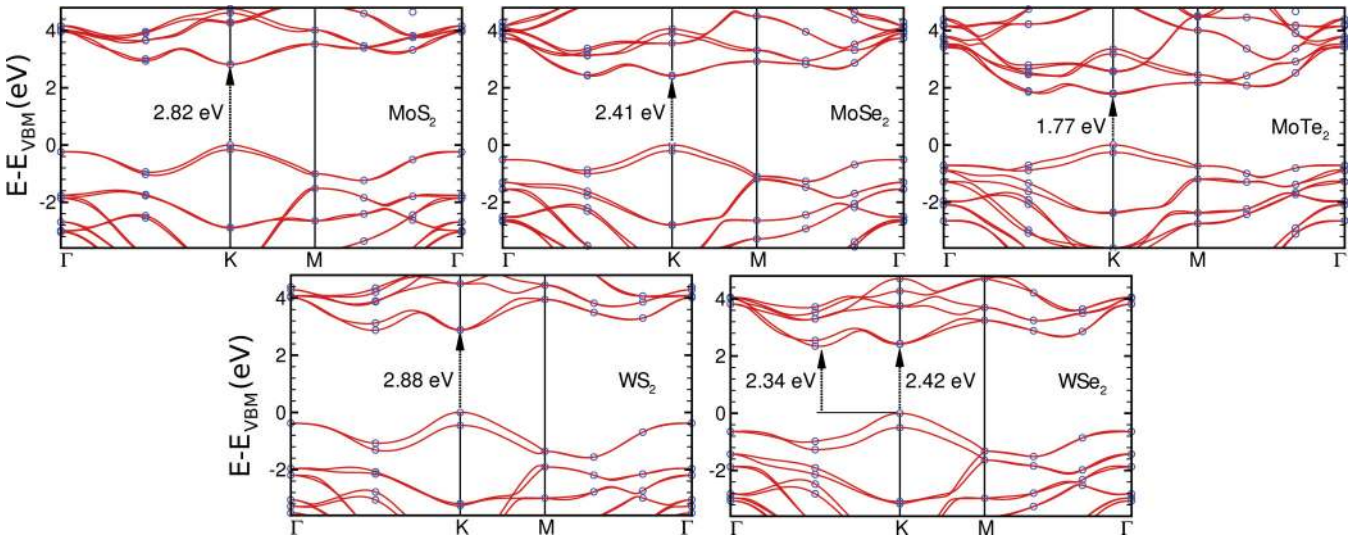

FIG. 3. (Color online) Quasiparticle band structures for MoX_2 and WX_2 monolayers obtained from Wannier interpolation. The energy at the valence-band maximum (E_{VBM}) is set to zero. Open circles correspond to k points that are explicitly sampled in the electronic structure calculation and are therefore not subject to any interpolation error. Quasiparticle gaps in all cases are direct at K with the exception of WSe_2, which has an indirect gap between the valence-band maximum at K and the conduction-band minimum at 0.52 Γ-K. Spin-orbit splitting of levels at the top of the valence band is clearly visible in all cases, the effect being particularly pronounced for the WX_2 compounds.

about three times smaller than that in the bulk ($\sim 14.5\epsilon_0$). The binding energy of the A exciton is then estimated to be $E_b^A = 0.85$ eV and the corresponding transition energy is $E_g^{G_0W_0} - E_b^A = 1.97$ eV, which is about 5%–10% in excess of the experimental and BSE values.

Having established the success of the computational strategy in describing the absorption spectrum of monolayer MoS_2, we now turn our attention to the remaining LTMDs. Figure 3 displays the quasiparticle band structures for the various monolayers studied here. As seen, all monolayers possess a direct gap at the K point with the sole exception of WSe_2, which has an indirect gap between the valence-band maximum at K and the conduction-band minimum located at 0.52 Γ-K.[40] The relaxed structural parameters for the monolayers are listed in Table I and are found to be in excellent agreement with previous studies.[21,34] As seen from these data, the lattice parameters and metal-chalcogen bond lengths are nearly insensitive to the choice of metal atom (Mo or W) but vary appreciably with the choice of chalcogen; heavier chalcogens lead to larger in-plane lattice constants and longer metal-chalcogen bonds. At the DFT level, the spin-orbit splitting at the top of the valence band (Table I) is in excellent agreement with previous calculations.[21] The spin-orbit splitting is sensitive to the level of theory employed, once again following the general trend $\Delta_{SO}^{PBE} < \Delta_{SO}^{G_0W_0} < \Delta_{SO}^{HSE}$. In general, the spin-orbit splitting is significantly enhanced in WX_2 monolayers as compared to the MoX_2 family;[21] in comparison, the choice of chalcogen within a particular family exerts a smaller influence on the spin-orbit splitting. Table I also lists the electronic band gaps at various levels of theory for all monolayers. As seen for both the MoX_2 and WX_2 families, heavier chalcogens are associated with smaller band gaps. On the other hand, switching the metal species while retaining the chalcogen (e.g., MoS_2 vs WS_2) has a comparatively smaller influence on the band gap.

Absorption spectra from BSE calculations for various LTMD monolayers are displayed in Fig. 4 and the relevant data listed in Table II, from which a few interesting trends are immediately noticeable. Within the MoX_2 or WX_2 families, we see a systematic redshift of the A and B exciton peaks as

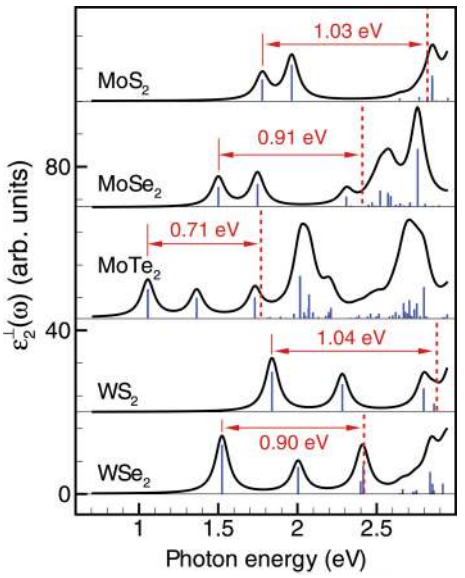

FIG. 4. (Color online) Imaginary part of the transverse dielectric constant $\epsilon_2^{\perp}(\omega)$ as a function of photon energy ($\hbar\omega$) for MoX_2 and WX_2 monolayers. Vertical (blue) bars represent the relative oscillator strengths for the optical transitions. Red dashed lines indicate the G_0W_0 band gap. Binding energies of the A exciton are indicated in each case.

the chalcogen species becomes heavier. While the effective exciton mass increases with heavier chalcogen species (Table II), the concomitant increase in dielectric screening is sufficient to lead to an systematic decrease in the exciton binding energy (recalling that $E_b \sim \mu_{ex}/\epsilon^2$). For a given chalcogen, the choice of metal atom has a smaller influence on the position of the A excitonic peak leading to fairly similar transition and exciton binding energies. This is not unexpected given the small variations in structural parameters, dielectric constants, band gaps, and carrier masses between MoS_2 and WS_2, as well as between $MoSe_2$ and WSe_2 (see Tables I and II). The position of the B excitonic peak is, however, quite sensitive to the choice of metal atom due to much larger spin-orbit coupling effects in W as opposed to Mo.[41] Nevertheless, the B excitons are also strongly bound, as may be inferred from Fig. 4. Overall, we conclude that all LTMD monolayers studied here universally display the presence of two strongly bound excitons below the direct band gap with excitation energies ranging from 1 to 2 eV, which would suggest possible optical applications in the near-IR to the red regime. In closing, we note that indirect (phonon-assisted) transitions, which are important only for WSe_2 here, are not included in the calculated absorption spectra. These phonon-assisted transitions will likely be present in room-temperature absorption and PL measurements. The direct quasiparticle gap at K and indirect gap between K and 0.52 Γ-K differ by about 80 meV; inclusion of phonon-assisted effects might therefore simply broaden and increase the weight of the first absorption peak, which should be kept in mind when comparing the computed spectrum with future experimental measurements on monolayer WSe_2.

In summary, state-of-the-art many-body GW and GW + BSE calculations were employed in this work to study the quasiparticle band structures and optical properties of MoX_2 and WX_2 monolayers. The presence of strongly bound excitons in monolayer MoS_2 was directly confirmed from these calculations and shown to be in excellent agreement with experimental measurements. Predictive simulations were performed for the remaining LTMDs to produce absorption spectra, which should be directly verifiable in future experiments. Overall, the absorption spectra of all monolayers studied here indicate the presence of two strongly bound excitonic peaks arising from vertical transitions at the K point from a spin-orbit-split valence band to a doubly degenerate conduction band. The exciton binding becomes weaker as the chalcogen becomes heavier, which may be understood in terms of the increased dielectric screening afforded by the more diffuse orbitals of heavier chalcogens. The exciton splitting in these materials is directly related to the magnitude of the spin-orbit splitting and is significantly enhanced in WX_2 compounds as compared to their MoX_2 counterparts. Excitation energies for these materials are predicted to range from 1 to 2 eV, which suggests potential applications in the near-IR to the red regime. As experimentss[9,11,19] on monolayer MoS_2 have already demonstrated, this class of materials ought to display strong photoluminescence upon thinning down to a monolayer due to an indirect-to-direct gap transition. Therefore, there is potential for tuning electronic and optical properties both via quantum confinement of carriers as well as by the chemical composition, which then offers promise for new optoelectronic applications. It is hoped that the results presented here will spur interest beyond MoS_2 and uncover rich physics in this family of materials.

ACKNOWLEDGMENTS

A.R. thanks Sahar Sharifzadeh and Doron Naveh for useful discussions and for a critical reading of this manuscript. Startup support from the University of Massachusetts, Amherst is gratefully acknowledged.

APPENDIX: COMPUTATIONAL METHODS

All calculations were performed with the Vienna *ab initio* package (VASP).[42] Core and valence electrons were treated using the projector-augmented wave (PAW) method.[43,44] The PAW potentials represent the nuclei plus core electrons up through the 3d shell for Mo and up through the 5s shell for W. For chalcogens, the s and p electrons of the outermost shell were treated as valence. The so-called GW version of the PAW potentials supplied with VASP were employed here for all atoms; these potentials are designed to provide improved scattering properties at high energies.[27] At the DFT level, electron exchange and correlation were treated using the generalized gradient approximation as parametrized by Perdew, Burke, and Ernzerhof.[30] Periodic images of monolayers were separated by at least 15 Å of vacuum, which is sufficient to ensure minimal interlayer coupling; importantly, this separation is sufficient to ensure that the longitudinal component of the macroscopic static dielectric tensor, $\epsilon^{||}_{\text{mac}}$, is close to unity. All atomic positions and cell vectors were relaxed with a tolerance of 0.01 eV/Å. Electronic minimization was performed with a tolerance of 10^{-4} eV and convergence accelerated with a Gaussian smearing of the Fermi surface by 0.05 eV. From convergence tests, the kinetic energy cutoff was set at 400 eV and the Brillouin zone sampled with a $6 \times 6 \times 1$ Γ-centered k-point mesh.

The self-consistent charge density from above was employed to perform a subsequent non-self-consistent spin-orbit coupling (SOC) calculation in the spirit of perturbation theory. A tighter electronic convergence criterion of 10^{-6} eV was employed from this point onward to ensure better convergence of unoccupied states. The converged SOC wave functions were then used as a starting point for a hybrid DFT calculation, which employed the Heyd-Scuseria-Ernzerhof (HSE) exchange-correlation functional.[31] Converged HSE eigenvalues and wave functions were in turn used to calculate quasiparticle energies in the non-self-consistent GW approximation (G_0W_0) as implemented in VASP.[27] It should be noted that only the quasiparticle energies are recalculated in a G_0W_0 calculation; the wave functions are not updated (remaining fixed at the HSE level). The quasiparticle energies and HSE wave functions were then employed to obtain the G_0W_0 band structure through Wannier interpolation using the WANNIER90 program.[45] In the final step, BSE spectra were obtained in the Tamm-Dancoff approximation using the VASP implementation. The four highest valence bands and the eight lowest conduction bands were used as a basis for excitonic

eigenstates, which is more than sufficient to converge the energies of the A and B peaks. For purposes of comparison, absorption spectra were also computed at the HSE and G_0W_0 levels within the random-phase approximation. A complex shift of $\eta = 0.05$ eV was applied in all optical calculations, which leads to a broadening of the theoretical absorption spectrum.

Finally, we note that while the additional hybrid-DFT step in the sequence of steps noted above is not essential (i.e., G_0W_0 + BSE calculations can be performed directly starting from PBE wave functions), the absorption peaks were found to be in better agreement with experiment when the HSE eigenvalues and eigenfunctions were employed for subsequent steps.

*ashwin@engin.umass.edu

[1] J. A. Wilson and A. D. Yoffe, Adv. Phys. **18**, 193 (1969).
[2] A. Enyashin, S. Gemming, and G. Seifert, Eur. Phys. J. Spec. Top. **149**, 103 (2007).
[3] M. Bar-Sadan, I. Kaplan-Ashiri, and R. Tenne, Eur. Phys. J. Spec. Top. **149**, 71 (2007).
[4] J. N. Coleman *et al*., Science **331**, 568 (2011).
[5] Z. Zhang, Z. Yin, X. Huang, H. Li, Q. He, G. Lu, F. Boey, and H. Zhang, Angew. Chem. Int. Ed. **50**, 11093 (2011).
[6] K. S. Novoselov, D. Jiang, F. Schedin, T. J. Booth, V. V. Khotkevich, S. V. Morozov, and A. K. Geim, Proc. Natl. Acad. Sci. USA **102**, 10451 (2005).
[7] H. S. S. Ramakrishna Matte, A. Gomathi, A. K. Manna, D. J. Late, R. Datta, S. K. Pati, and C. N. R. Rao, Angew. Chem. Int. Ed. **49**, 4059 (2010).
[8] A. Ayari, E. Cobas, O. Ogundadegbe, and M. S. Fuhrer, J. Appl. Phys. **101**, 014507 (2007).
[9] K. F. Mak, C. Lee, J. Hone, J. Shan, and T. F. Heinz, Phys. Rev. Lett. **105**, 136805 (2010).
[10] B. Radisavljevic, A. Radenovic, J. Brivio, V. Giacometti, and A. Kis, Nat. Nanotechnol. **6**, 147 (2011).
[11] A. Splendiani, L. Sun, Y. Zhang, T. Li, J. Kim, C.-Y. Chim, G. Galli, and F. Wang, Nano Lett. **10**, 1271 (2010).
[12] B. Radisavljevic, A. Radenovic, J. Brivio, V. Giacometti, and A. Kis, Nat. Nanotechnol. **6**, 147 (2011).
[13] B. Radisavljevic, M. B. Whitwick, and A. Kis, ACS Nano **5**, 9934 (2011).
[14] Z. Yin, H. Li, H. Li, L. Jiang, Y. Shi, Y. Sun, G. Lu, Q. Zhang, X. Chen, and H. Zhang, ACS Nano **6**, 74 (2012).
[15] T. Böker, R. Severin, A. Müller, C. Janowitz, R. Manzke, D. Voss, P. Kruger, A. Mazur, and J. Pollmann, Phys. Rev. B **64**, 235305 (2001).
[16] A. Klein, S. Tiefenbacher, V. Eyert, C. Pettenkofer, and W. Jaegermann, Phys. Rev. B **64**, 205416 (2001).
[17] T. Li and G. Galli, J. Phys. Chem. C **111**, 16192 (2007).
[18] S. Lebègue and O. Eriksson, Phys. Rev. B **79**, 115409 (2009).
[19] G. Eda, H. Yamaguchi, D. Voiry, T. Fujita, M. Chen, and M. Chhowalla, Nano Lett. **11**, 5111 (2011).
[20] T. Cheiwchanchamnangij and W. R. L. Lambrecht, Phys. Rev. B **85**, 205302 (2012).
[21] Z. Y. Zhu, Y. C. Cheng, and U. Schwingenschlögl, Phys. Rev. B **84**, 153402 (2011).
[22] A. Ramasubramaniam, D. Naveh, and E. Towe, Phys. Rev. B **84**, 205325 (2011).
[23] G. Onida, L. Reining, and A. Rubio, Rev. Mod. Phys. **74**, 601 (2002).
[24] L. Hedin, Phys. Rev. **139**, A796 (1965).
[25] M. S. Hybertsen and S. G. Louie, Phys. Rev. B **34**, 5390 (1986).
[26] R. W. Godby, M. Schluter, and L. J. Sham, Phys. Rev. B **37**, 10159 (1988).
[27] M. Shishkin and G. Kresse, Phys. Rev. B **74**, 035101 (2006).
[28] M. Rohlfing and S. G. Louie, Phys. Rev. Lett. **81**, 2312 (1998).
[29] S. Albrecht, L. Reining, R. del Sole, G. Onida, Phys. Status Solidi A **170**, 189 (1998).
[30] J. P. Perdew, K. Burke, and M. Ernzerhof, Phys. Rev. Lett. **77**, 3865 (1996).
[31] J. Heyd, G. E. Scuseria, and M. Ernzerhof, J. Chem. Phys. **118**, 8207 (2003); **124**, 219906 (2006).
[32] B. G. Janesko, T. M. Henderson, and G. E. Scuseria, Phys. Chem. Chem. Phys. **11**, 443 (2009).
[33] E. N. Brothers, A. F. Izmaylov, J. O. Normand, V. Barone, and G. E. Scuseria, J. Chem. Phys. **129**, 011102 (2008).
[34] P. Johari and V. B. Shenoy, ACS Nano **5**, 5903 (2011).
[35] R. Coehoorn, C. Haas, J. Dijkstra, C. J. F. Flipse, R. A. de Groot, and A. Wold, Phys. Rev. B **35**, 6195 (1987).
[36] J. K. Ellis, M. J. Lucero, and G. E. Scuseria, Appl. Phys. Lett. **99**, 261908 (2011).
[37] M. Grüning, A. Marini, and X. Gonze, Nano Lett. **9**, 2820 (2009).
[38] G. Grosso and G. Pastori-Parravicini, *Solid State Physics* (Academic Press, London, 2000).
[39] M. Shinada and S. Sugano, J. Phys. Soc. Jpn. **21**, 1936 (1966).
[40] At the PBE and HSE levels, the fundamental gap for WSe_2 is direct at K. The reason for the shift in the conduction-band minimum to 0.52 Γ-K in the G_0W_0 calculation is unclear; additional calculations at the partially self-consistent GW_0 or fully self-consistent GW level are planned in future work to probe this issue.
[41] It should be noted that the exciton splitting is not exactly equal to the valence-band spin-orbit splitting at K due to differences in binding energies for the A and B excitons.
[42] G. Kresse and J. Furthmüller, Comput. Mater. Sci. **6**, 15 (1996); Phys. Rev. B **54**, 11169 (1996).
[43] P. E. Blochl, Phys. Rev. B **50**, 17953 (1994).
[44] G. Kresse and D. Joubert, Phys. Rev. B **59**, 1758 (1999).
[45] A. A. Mostofi, J. R. Yates, Y.-S. Lee, I. Souza, D. Vanderbilt, and N. Marzari, Comput. Phys. Commun. **178**, 685 (2008).